Cement and Concrete Research 85 (2016) 12–27

Contents lists available at ScienceDirect

Cement and Concrete Research

journal homepage: www.elsevier.com/locate/cemconres

Elemental zonation in marine concrete

Ulla Hjorth Jakobsen [a], Klaartje De Weerdt [b,*], Mette R. Geiker [b]

[a] Danish Technological Institute, Taastrup, Denmark
[b] NTNU, Department for Structural Engineering, Trondheim, Norway

ARTICLE INFO

Article history:
Received 7 August 2015
Accepted 9 February 2016
Available online 12 April 2016

Keywords:
Chloride (D)
Sulphate attack (C)
Microstructure (B)
Carbonation (C)
Sulphate resistant cements (D)

ABSTRACT

This paper presents a large collection of microstructural studies on concretes exposed to marine environments for periods between 2 and 34 years. The phase changes were studied using optical as well as scanning electron microscopy. A total of 21 concretes, taken from 9 different locations along the Norwegian and Danish coastlines, were investigated. Chemical zonation and mineralogical zonation were observed in the surface regions of marine-exposed concrete. Three zones were found irrespective of the age, location or binder composition: a magnesium-rich zone, a sulfur-rich zone, and a chlorine-rich zone. The absence of major damage indicates that the observed phase changes led only to minor scaling. This suggests that, rather than sulfate attack, sea water merely causes sulfur enrichment.

© 2016 The Authors. Published by Elsevier Ltd. This is an open access article under the CC BY-NC-ND license (http://creativecommons.org/licenses/by-nc-nd/4.0/).

1. Introduction

Reinforced concrete is commonly used as a construction material for structures exposed to sea water such as bridges and piers. The service life of these structures is generally limited by chloride-induced reinforcement corrosion. Chlorides originating from the sea water penetrate the concrete cover and cause pitting corrosion in the reinforcement when they exceed a critical level.

The extent of chloride ingress in concrete is generally investigated by determining chloride profiles and evaluating the chloride concentration at the depth of the reinforcement. The chloride profiles give the total chloride content in the concrete at different depths from the exposed surface. In concrete, chlorides can be bound in calcium chloroaluminate hydrates, such as Friedel's salt or Kuzel's salt, they can be adsorbed onto calcium silicate hydrate (C–S–H), and they can be present in the pore solution.

Chlorides are by themselves not harmful to concrete. However, what is often neglected is that, in addition to chloride and its main associated cation sodium, sea water also contains other ions which are potentially aggressive for the concrete itself, such as magnesium, sulfate and carbonate ions. These ions influence the chloride ingress either by affecting the chloride-binding capacity of the paste, by affecting the porosity of the concrete cover, or by causing the concrete cover to deteriorate.

The sulfate in sea water can lead to the formation of gypsum by reacting with the calcium hydroxide, or ettringite through reaction with the aluminate phases. The reaction with sulfate can potentially lead to cracking [1]. However, the cracking of concrete due to sulfates originating from sea water appears to be limited [2,3]. The presence of sulfate also reduces the chloride-binding capacity of the paste [4–6].

The magnesium present in sea water can precipitate as brucite when it meets the high pH of the concrete [7], or it can also react with decalcified C–S–H to form the non-cementing magnesium silicate hydrate (M–S–H) [8]. This magnesium-rich zone near the surface is weak and might not be observed in field samples due to its removal by abrasion [9].

In a marine environment, concrete is also exposed to carbonates. The carbonates can originate from the sea water or from the air. In addition to depositing as a calcium-carbonate crust on the outer surface, carbonates can also react with the calcium ions present in the pore solution to form calcium carbonate in the concrete close to the surface. The formation of a calcium-carbonate-crust might have a sealing effect on the concrete surface. Moreover, carbonates within the paste reduce the chloride-binding capacity of the cement paste [4,5].

At temperatures below 15 °C, exposure to sulfate from sea water on concrete containing calcium carbonate (for example, as limestone filler) or combined sulfate and carbonate exposure on concrete can result in the conversion of C–S–H into thaumasite [10,11]. Thaumasite is a non-cementing reaction product which can result in disintegration that causes scaling of the concrete.

In addition to the effects of sulfate, carbonate and magnesium ions, sea water will also affect the hydrate composition of the concrete due to leaching. Sea water tends to leach out hydroxyl and calcium ions from the hydrated cement paste, resulting in the dissolution of Portlandite and the decalcification of C–S–H.

Table 1 shows the composition of sea water in the Atlantic, the Trondheim Fjord and the Baltic Sea. Note that the total salt concentration in sea water can vary, for example due to fresh water dilution from rivers, but the proportions of the constituents are essentially

* Corresponding author: Tel.: +47 93 65 66 33.
E-mail address: Klaartje.d.weerdt@ntnu.no (K. De Weerdt).

http://dx.doi.org/10.1016/j.cemconres.2016.02.006
0008-8846/© 2016 The Authors. Published by Elsevier Ltd. This is an open access article under the CC BY-NC-ND license (http://creativecommons.org/licenses/by-nc-nd/4.0/).

Table 1
Concentrations of the main elements in sea water from the Atlantic Ocean [47], Trondheim Fjord [15] and the Baltic Sea [48].

Conc. [mg/l]	Cl	Na	Mg	S	Ca	K	C
Atlantic	19,000	10,500	1350	890	400	380	28
Trondheim Fjord	21,100	10,990	1330	990	430	380	20
Baltic Sea	3,900	2,140	260	570	50	70	–

constant. Also, the sea is a relatively endless reservoir compared to the concrete structure it is in contact with. It might thus be expected that the combined chemical impact of the different ions present in sea water is general for marine-exposed structures.

The above points show that the effect of sea water on the phase assemblage of concrete is complex due to the presence of such a variety of ions in sea water. Duval et al. [12] pointed out that differences in the mobility of the aggressive ions and in the solubility of the reaction products cause their combined impact to result in zonation near the concrete surface.

Few studies have been published on the effect of zonation caused by the different ions present in sea water on concrete structures, among them are Marchand et al. [13], Chabrelie et al. [14], Jakobsen et al. [9] and De Weerdt et al. [15].

This paper presents a microstructural study on the zonation caused by sea water. The data set comprises 21 different concretes exposed to sea water in 9 different locations with exposure times ranging from 2 to 34 years. This large data set allows the identification of common features and discussion of typical microscopic morphologies of phases arising from sea water exposure. Three zones were found irrespective of the age, location and binder composition: a magnesium-rich zone, a sulfur-rich zone, and a chlorine-rich zone. The absence of major damage suggests that, rather than sulfate attack, sea water merely causes sulfur enrichment.

2. Experimental

2.1. Materials

The concretes examined are from marine-exposed trial elements and concrete structures in Denmark and Norway (Fig. 1). They include recently cast concrete subjected to sea water for only 2 years, and concrete subjected to sea water for up to 34 years (Table 2).

The short-term exposed concretes are Danish trial concrete elements made for studies for the coming Fehmarn Belt fixed link between Denmark and Germany [9]. The concretes were cast in the laboratory of the Danish Technological Institute and contain different binder combinations; an overview of mix designs and exposure conditions is given in Table 2. The concrete ID reflects the binder composition, location and exposure time; CEM Is stands for sulfate resistant Portland cement, CEM I for Portland cement, FA for fly ash, SF for silica fume, L for limestone. Two types of elements were produced: panels and cylinders. They were all demoulded after 24 h. The panels were kept sealed until exposure, while the cylinders were cured under saturated conditions until a couple of days before exposure, when they were surface-dried and their curved surfaces were sealed with epoxy. The panels and cylinders were exposed to sea water at Rødby Havn on the south coast of Denmark (Fig. 1) at the age of around 40 maturity days. The temperature was measured by thermo couples inserted in the concrete and the maturity was calculated using the method by Freiesleben [16]. The concrete cylinders were put in cages submerged in sea water at a level of −1.5 m, while the panels were kept only partly submerged in sea water (averaging −0.1 m under water level, at the bottom of the tidal zone ±0.15 m). At different time intervals, the cylinders were taken out of the cages and cores were drilled from the panels. The results presented in this paper are from specimens taken at an exposure age of 2 years [9].

The Danish long-term exposed concretes studied are from five major marine bridges: the Vejle Fjord Bridge, the Farø Bridges, the Alssund Bridge, the Storstrøm Bridge, and the Øresund Bridge. These structures are all located in the southern, inner waters of Denmark (Fig. 1). Cores from the structures were taken below the average water level, except for the Øresund Bridge where cores were also taken above the average water level (Table 2). All cores were taken from visually intact areas; i.e. without coarse cracking or macroscopical scaling.

The Norwegian concretes are from trial elements at two exposure sites (Fig. 1). After 1 week of curing, a concrete panel was exposed for approximately 10 years at Østmarkneset in the tidal zone of Trondheim Fjord. The second series had been exposed for 16 years partly submerged on the west coast of Norway at Solsvik near Bergen after

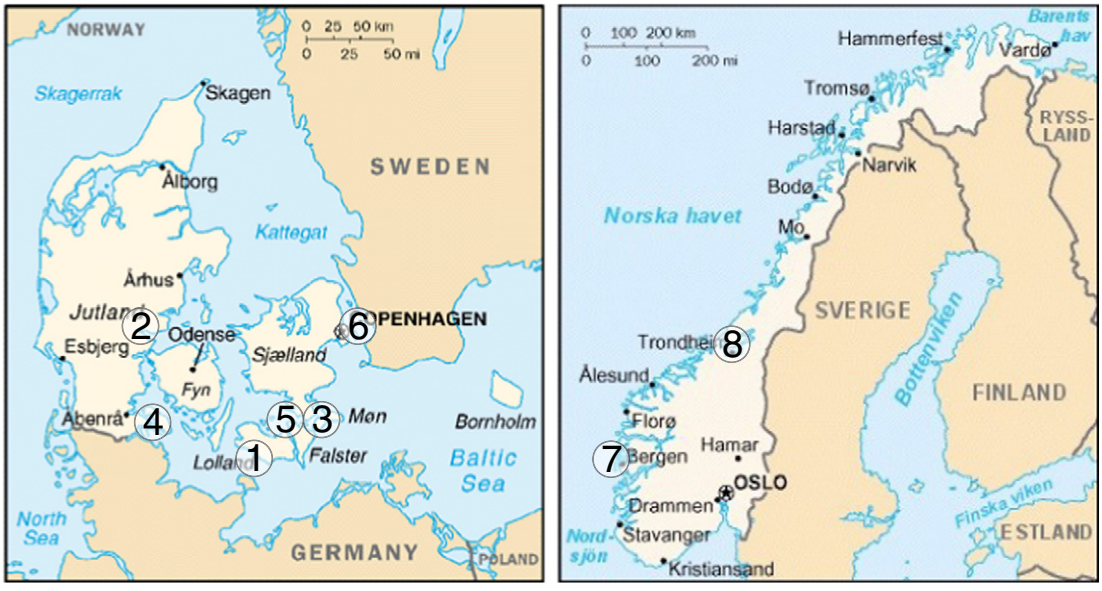

Fig. 1. Locations: (1) Rødby Havn Fehmarn exposure site, (2) Vejle Fjord Bridge, (3) the Farø Bridges, (4) the Alssund Bridge, (5) Storstrøm Bridge, (6) the Øresund Bridge, (7) Solsvik exposure site, and (8) Østmarkneset exposure site.

Table 2
Concrete compositions from mix design [in kg/m^3 unless otherwise stated] and exposure conditions.

	Short-term exposure									Long-term exposure								
	DK									DK					NO			
	Fehmarn									Bridges					Solvik and Østmarkneset			
Structures	Trial panels						Cylinders			Vejle Fjord	Farø	Alssund	Storstrøm	Øresund[a]	Solsvik			Østm
Concrete ID [b]	CEM Is Feh 2y	CEM Is + 15%FA Feh 2y	CEM Is + 25%FA Feh 2y	CEM Is + 4%SF Feh 2y	CEM Is + 12%FA + 4%SF Feh 2y	CEM III/B Feh 2y	CEM II/A L Feh 2y	CEM I Feh 2y	CEM I + 30%FA Feh 2y	CEM III/B Vej 34y	CEM Is + 11%FA Far 30y	CEM Is Als 31y	CEM Is Sto 75y	CEM Is + 5%SF Øre 12y	CEM I + 8%SF Sol 16y	CEM III/B + 4%SF Sol 16y	CEM I + 19%FA + 4%SF Sol 16y	CEM I + 10%L Øst 10y
CEM I 42.5 N SR	365	322	320	340	340						330		x[c]					
CEM I 42.5R SR														≤300				
CEM I SR[d] (DK ALS)												335						
CEM I 42.5R																		366
CEM I 52.5 N								365	280						378		339	
CEM II/A LL 52.5R							365											
CEM II/BS 52.5 N																394		
CEM III/B 42.5 N SR						360				400								
Fly ash (FA)		57	107		49				120		40						84	
Silica fume (SF)				14	16									≥15	34	16	17	
Limestone (L)							x											44
Water	146	140	149	147	159	144	146	146	136	180	150	–	–	–	181	165	186	171
Sand	705	671	694	695	696	689	691	693	642	670	580	–	–	–	872	889	795	1053
Aggregates	1189	1182	1077	1172	1081	1161	1165	1169	1181	1130	1149	–	–	–	898	920	926	688
w/(c + 2 SF + 0.5 FA)	0.40	0.40	0.40	0.40	0.40	0.40	0.40	0.40	0.40	0.45	0.45	-	-	0.40	0.41	0.39	0.45	0.42
w/b	0.40	0.37	0.35	0.42	0.39	0.40	0.40	0.40	0.34	0.45	0.41	-	-	0.40	0.44	0.40	0.42	0.42
Exposure [e]	bw	bw	bw	bw	bw	bw	bw	bw	bw	bw	bw	bw	bw	aw/bw	bw	bw	bw	spl
Average below-water level [m]	−0.1	−0.1	−0.1	−0.1	−0.1	−0.1	−1.5	−1.5	−1.5	−1.0	−1.5	−1.5	–	–	−1.0	−1.0	−1.0	–
Years of exposure	2	2	2	2	2	2	2	2	2	34	30	31	75	12	16	16	16	10

[a] Several different locations.
[b] In the concrete ID the binder composition, location and exposure time are reflected, regarding the binder CEM Is stands for sulfate resistant Portland cement, CEM I for Portland cement, FA for fly ash, SF for silica fume, L for limestone.
[c] CEM I with unknown amount and composition.
[d] Special early Danish SR cement.
[e] ab = above water, bw = below water, spl = splash zone.

2 months of curing outdoors sheltered from sea water. The cores were retrieved from the submerged parts of the three elements.

The Norwegian concretes were exposed to the open salt water of the Atlantic, while the Danish concretes were exposed to the more fresh water-influenced water of the Baltic Sea (Fig. 1). All the concretes studied were exposed to relatively cold sea water with similar chemistry, but with very different concentrations (Table 1). All concrete surfaces were to some extent exposed to abrasion as well as biological growth.

It should be noted that the binders used for the Fehmarn trial panels and the long-term exposed Danish bridges are categorized as sulfate resistant according to EN 197 [17], whereas the binders for the Fehmarn cylinders and Norwegian concretes are not (see Table 2).

The oxide composition of the cements and supplementary cementitious materials used for the Fehmarn concretes, and the Solsvik and Østmarkneset concretes are given in Table 4 and Table 5, respectively. For the older concretes the compositions of the cements could not be retrieved. As the degree of reaction of the binders is unknown the oxide composition will not be referred to in the discussion.

2.2. Sample preparation

The data reported in this paper is based on the examination of fluorescent epoxy impregnated thin sections and polished sections. The chloride ingress data from beyond the depth of the thin sections was measured using titration on a companion sample [18].

The preparation techniques used are described by Jakobsen et al. and Detwiler et al. [19,20]. All samples for SEM–EDS analysis were prepared using ethanol instead of water in order to minimize the interaction with unhydrated and hydrated phases. The preparation technique involved drying of samples, which could lead to precipitation of secondary phases, even though this was not observed. The temperature during the drying process did not exceed 35 °C. The epoxy used for impregnation of the concrete specimens contained a small amount of chloride, but based on background levels we considered this amount too small to influence the chloride content measured in the concrete.

2.3. Optical microscopy

Thin sections were analyzed using a Leica DM2500P optical polarizing microscope equipped with a fluorescent facility. The fluorescent filter combination used was a BG12 excitation filter and a K530 yellow blocking filter.

This analysis reveals information about e.g. aggregates, paste composition and homogeneity, and allows observation of cracks and defects down to less than 10 μm. In this study, optical microscopy was especially used to detect the extent and spatial distribution of carbonation, capillary porosity and secondary precipitated phases in voids and cracks [19].

2.4. SEM–EDS

Polished sections were examined in a Quanta 400 ESEM from FEI equipped with a Thermo SNN EDS analysis unit operated at high vacuum mode at an accelerating voltage of 20 keV and a spot size of 5. The samples were carbon-coated. The analysis programme was set up to analyze the following elements: Na, Mg, Al, Si, S, P, Cl, K, Ca, Mn, Ti and Fe. Oxygen was calculated as difference. The data have been ZAF-corrected.

During analysis, chemical line traverses from the surface to a depth of about 30–120 mm were obtained by analyzing selected areas measuring 10 × 10 μm of the outer hydration (OH) products. OH products are defined as products formed outside the original cement grains. Cracks and aggregates were avoided during area selection. Crystalline phases formed in voids, e.g. relicts of cement grains, were analyzed separately and the results were included in dot plots, but not in the line traverses. The analysis steps in the line traverse were 20 μm in the outer 100 μm, followed by steps of 100 μm until a depth of 1 mm, then 1 mm steps to 5 mm, 2.5 mm steps to 20 mm, and finally steps of 10 mm until the maximum depth of the specimen.

In order to delimit elevated concentrations of elements and their extent of penetration and/or movement near the sea water exposed surface, background levels of the cement paste were calculated based on the content of the given elements in non-affected areas of the concrete (not from the chemistry of the cement, as this was not available for all used cements). In this study the background value for Na is considered to be below 1 at.%, Mg approximately below 1 at.% (a bit different for the slag concretes), S below 1–2 at.% and Cl below 1 at.%.

EDS results are presented both as profiles in atomic mass % (see Fig. 2), with the focus on chlorine, magnesium and sulfur profiles, and in dot plots (see Fig. 5). During EDS analysis, a certain paste volume comprising a mixture of phases is analyzed. An EDS dot plot depicts the ideal composition of phases likely to form in the paste. An EDS analysis of a paste volume comprising a mixture of phases will lie within the ideal composition of these phases.

3. Results and discussion

As mentioned earlier, all cores were taken from visually intact areas. The microscopic investigations revealed, however, that most of the surfaces were partly microscopically scaled, and that the exposed surface of concrete cores from three of the long-term exposed Danish bridges were scaled before the later formation of a calcite crust, see Table 3.

3.1. Zonation

All the concretes examined showed the same type of zonation of the surface region. This zonation relates to sea water ingress. The zonation is

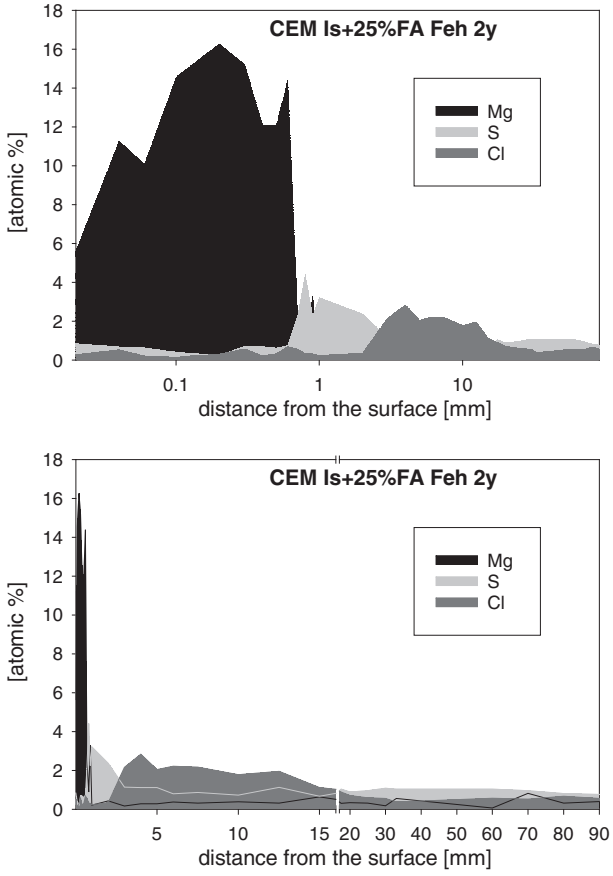

Fig. 2. Typical zonation observed in concrete exposed to sea water. The example is from the CEM Is + 25%FA Feh 2y concrete exposed submerged for 2 years at Rødby Havn, Denmark.

Table 3
Phases observed in the light microscope and observation of microscopic surface scaling for the various concretes tested.

Structures	Short-term exposure										Long-term exposure									
	DK										DK					NO				
	Fehmarn										Bridges					Solvik and Østmarkneset				Østm.
	Panels					Cylinders					Vejle Fjord	Farø	Alssund	Storstrøm	Ørresund[a]	Solsvik				
Concrete ID	CEM Is Feh 2y	CEM Is + 15%FA Feh 2y	CEM Is + 25%FA Feh 2y	CEM Is + 4%SF Feh 2y	CEM Is + 12%FA + 4%SF Feh 2y	CEM III/B Feh 2y	CEM II/A L Feh 2y	CEM I Feh 2y	CEM I + 30%FA Feh 2y		CEM III/B Vej 34y	CEM Is + 11%FA Far 30y	CEM Is Als 31y	CEM Is Sto 75y	CEM Is + 5%SF Øre 12y	CEM I + 8%SF Sol 16y	CEM III/B + 4%SF Sol 16y	CEM I + 19%FA + 4%SF Sol 16y	CEM I + 10%L Øst 10y	
Calcite crust		X					(X)	(X)	(X)			**X**	**X**	**X**		X	X	X	(X)	
Brucite in calcite crust		X											X		X	X	X		X	
Brucite in cracks																			X	
Mg freckles																				
M–S–H	X	(X)	X	X	X	X	X	X	X			X	X	X	X	X	(X)	(X)	X	
Gypsum in voids			X	X	X	X	X	X	X							X				
Thaumasite in voids				X	X		X	X	X			X	X						X	
Partly microscopically scaled surface	X	X		X			X	X	X										X	
Microscopically scaled surface			X		X	X					X	X	X	X						
Intact surface															X			X		
Exposed aggregates											X	X	X							

[a] Several different locations; (X) occasionally seen; X formed on earlier microscopically scaled surfaces.

Table 4
Oxide composition of the cements and supplementary cementitious materials used for the Fehmarn concretes, except for the CEM II/A LL 52.5R of which the composition is not available.

	CEM I 42.5 N SR	CEM I 52.5 N	CEM III	Fly ash	Blast furnace slag	Silica fume
SiO_2	24.84	20	30.3	60.34	33.5	95.4
Al_2O_3	2.91	5.34	9.44	20.46	12.95	
Fe_2O_3	2.34	3.78	0.74	7.39	0.4	1.5
CaO	65.61	63.4	47.8	2.03	40.09	0.32
MgO	0.75	0.86	4.88		8.09	
SO_3	2.2	3.3	2.5	0.5	2.7	0.23
K_2O						0.8
Na_2O						0.19

illustrated in Fig. 2, which shows the elemental profiles for magnesium, sulfur and chlorine as a function of depth from the exposed surface for one of the Fehmarn concretes with 25% fly ash, which had been submerged in sea water for 2 years. Based on the elemental changes, one can distinguish the three zones:

- the magnesium-rich zone,
- the sulfur-rich zone, and
- the chlorine-rich zone.

The zones more or less follow each other, but typically, a slight overlap between the sulfur-rich and the chlorine-rich zones can be observed. The zonation of the different concretes investigated is shown in the bar diagrams in Fig. 3. Based on the diagrams it can already at this stage be concluded that the order of the zones is independent of age, location, and binder composition.

Figs. 4 and 5 show the EDS dot plots for all EDS analysis performed, both on the outer hydration product (OH) and on the crystalline phases confined in voids, at different depths for all the different samples. These plots allow the identification of sulfur- or chlorine-containing phases, such as ettringite, Friedel's salt, and thaumasite.

Fig. 6 gives a schematic overview over the zonation near the concrete surface due to marine exposure as well as the corresponding elemental profiles and the observations made using SEM–EDS and light microscopy. In the following, these profiles are correlated with microstructural observations in relation to both the morphology and the composition of the phases.

3.2. Capillary porosity

Most of the concretes, which are microscopically scaled (Table 3) at the surface, typically showed an increased capillary porosity close to the

Table 5
Oxide composition of the cements and supplementary cementitious materials used for the Solsvik and Østmarkneset concretes.

	CEM I 52.5 N[a]	CEM I 42.5 N[b]	CEM I 42.5 R[c]	SF[d]	FA	slag
SiO_2	21.3	20.8	19.79	95.1	55.4	34.1
Al_2O_3	4.1	5.2	4.73	1	27.4	14.6
Fe_2O_3	3.2	2.9	3.25	0.1	3.9	0.5
CaO	64.3	63.7	62.02	0.1	3.6	41.4
MgO	1.7	2.6	2.37	0.4	1	7.7
SO_3	2.9	2.8	3.0	0.0		2.4[e]
K_2O	0.4	0.7	1.0	1.0	1.1	
Na_2O	0.2	0.3	0.3	0.1	0.3	

[a] Used for SF and FA containing concrete at Solsvik.
[b] Used for slag containing concrete at Solsvik.
[c] Used for the Østmarkneset concrete.
[d] General composition, not of the specific batch used.
[e] Recalculated from the S^{2-} content.

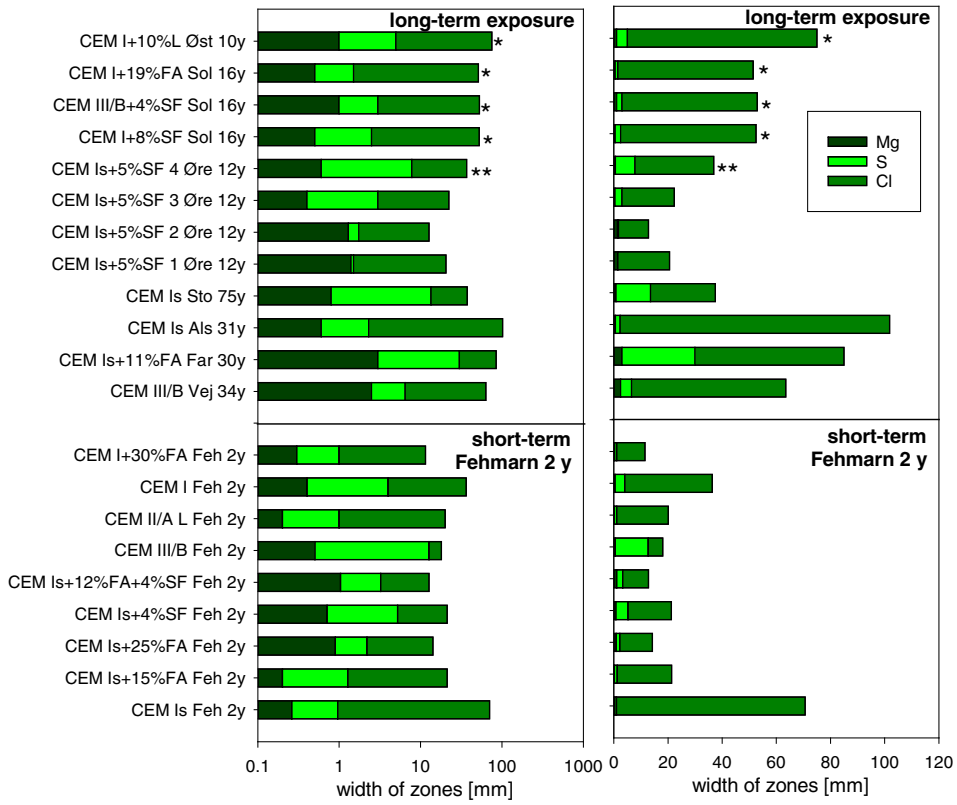

Fig. 3. Bar diagrams showing in logarithmic (left) and linear (right) scales the extent of the zones in the concretes with long-term and short-term exposures. The samples from Øresund (CEM Is + 5%SF Øre 12y) represent concretes from below water level (1–3) and above water level (4). (*) indicates that the end of the chloride-rich zone was determined by titration; (**) indicates high chloride at the end of the section.

exposed surface compared to the interior. When the concrete surface, however, was covered by a dense calcite crust, as in the Norwegian concretes from Solsvik, no increase in paste porosity was observed.

Fig. 7 shows the depth of the zone with increased capillary porosity determined by light microscopy alongside the depth of the magnesium and sulfur zone for a selection of the concretes. The deepest levels of increased porosity are observed in the long-term exposed concretes, where increased porosity occured to depths of between 6 and 13 mm. In the short-term exposed concretes, increased porosity is observed at depths of up to 4 mm. The data indicates that there is no direct relationship between the porosity and the elemental changes (sulfur and magnesium).

Sulfur and magnesium ingress will result in an increase in the volume of solids. This might compensate for the loss of solids by leaching. For most of the concretes, the magnesium and sulfur-rich zones lie within the zone with increased porosity, which indicates that the volume of the sulfur and magnesium phases is insufficient to compensate for the leaching.

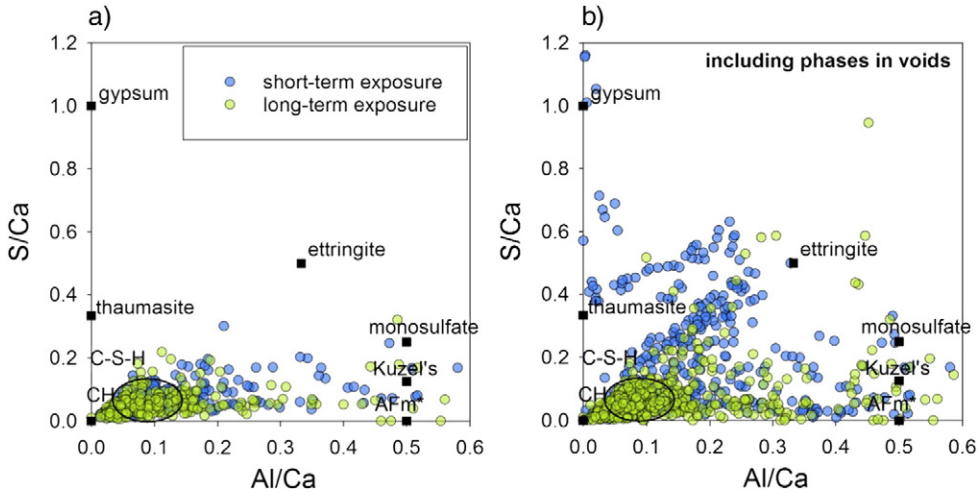

Fig. 4. EDS dot plots for the concretes examined. The plots allow the identification of the sulfur-containing phases: a) shows the results for the OH products, and b) includes the phases precipitated in voids. (AFm* represents AFm phases without sulfur, e.g. Friedel's salt and monocarbonate).

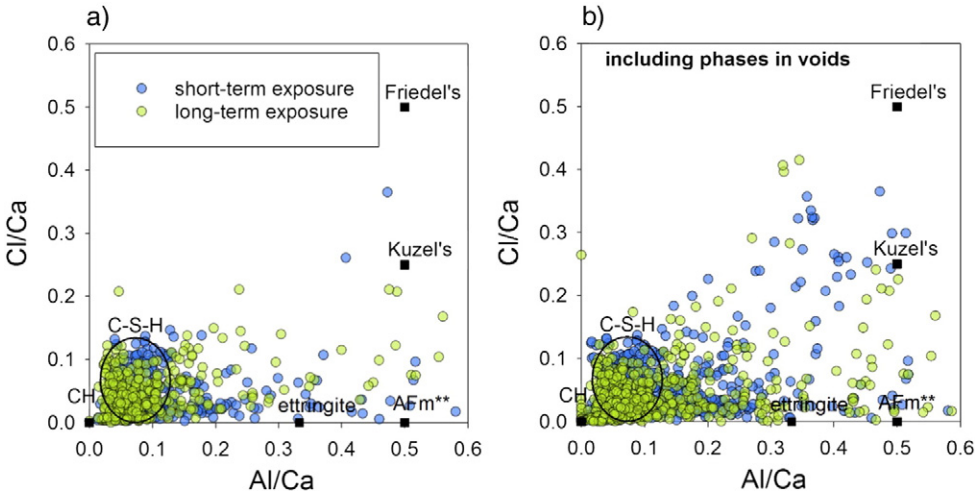

Fig. 5. EDS dot plots for the concretes examined. The plots allow the identification of the chlorine-containing phases: a) shows the results for the OH products, and b) includes the phases precipitated in voids. (AFm** represents AFm phases without chlorine, e.g. monosulfate and monocarbonate).

3.3. Carbonate phases

A simplified chemical reaction for the formation of calcium carbonate is given in Eq. 1.

$$H_2CO_{3(aq)} + Ca(OH)_{2(s)} \rightarrow CaCO_{3(s)} + 2H_2O_{(l)} \quad (1)$$

On several of the concrete surfaces, intact as well as microscopically scaled, a thin dense crust of calcite was observed (see Fig. 9 and Table 3). An intact calcite crust was observed on all four Norwegian concretes; as well as on one of the short-term exposed panels (CEM Is + 15%FA Feh 2y) and on earlier scaled surfaces of three cores from long-term exposed Danish concrete (Farø, Alssund, Storstrøm). Partial coverage by calcite was observed on the surface of three short-term exposed cylinders; whereas no calcite was observed on the exposed surface of the remaining concretes. The thin crust of calcite often encapsulates shell fragments of molluscs and other organisms. The carbonates involved in the crust formation can originate from the sea water or, in the case of not fully submerged concrete, from the air. Buenfeld and Newman [7] observed the formation of a 50–100 μm thick aragonite ($CaCO_3$) layer on concrete submerged in sea water in laboratory conditions.

In addition to depositing as a crust on the outer surface, carbonates can also react with the calcium-containing phases present in the cement paste to form calcium carbonate, the so-called carbonation. The carbonation process should be distinguished from the formation of the calcite crust, as carbonation is a replacement process while crust formation is a precipitation process. In the outermost millimeter of the concrete under the calcite crust, the paste is typically patchy carbonated and any air voids may be partly filled with calcite (see Fig. 16). Fig. 8 gives the extent of carbonation determined by light microscopy in the samples investigated.

A distinct morphology of calcite, which is known as popcorn carbonation, is typically observed between the Mg-rich and the S-rich zones, or right beneath the calcite crust (see Fig. 10). Popcorn carbonation is a special form of carbonation in which the C–S–H gel "splits" up into relatively large calcite clusters that look like popcorn with a decalcified interstitial silicate-rich gel phase often containing traces of Na and K. Several authors report popcorn carbonation occurring in cases where the water contains carbonic acid, e.g. Sibbick et al. and Thaulow et al. [10,21].

3.4. Magnesium phases

The magnesium present in sea water can precipitate as brucite ($Mg(OH)_2$) when it comes into contact with the highly alkaline pore solution of concrete (Eq. (2)). In its normal pH range, sea water is undersaturated with respect to brucite by at least two orders of magnitude. When sea water reaches a pH greater than 9.4, it will become saturated with respect to brucite [7].

$$Mg^{2+}_{(aq)} + Ca(OH)_{2(s)} \rightarrow Mg(OH)_{2(s)} + Ca^{2+}_{(aq)}. \quad (2)$$

Brucite precipitates on concrete surfaces exposed to sea water. In some of the investigated sections, brucite was observed as part of the crust together with calcite, and filling of cracks connected to the exposed surface (see Fig. 11 and Table 3). Fig. 12 shows a BSE image and magnesium map of the Norwegian concrete from Østmarkneset. It can be seen that a crack connected to the exposed surface is filled with a magnesium-rich phase, which was identified as brucite using SEM–EDS.

Brucite as such was not observed in the cement paste. Analysis of the magnesium-enriched zone in the outer cement paste indicates that this zone mainly consists of M–S–H (magnesium silicate hydrate). In the literature, there are very few records of the observation of M–S–H in marine-exposed concrete [8,9,13,22]. The reason for this might be that this magnesium-rich zone, which is very thin and weak, is eroded due to its inferior mechanical properties [13]. M–S–H is more commonly observed in concrete exposed to $MgSO_4$ [11,23–26] and $MgCl_2$ solutions [27,28], as well as in concrete exposed to saline ground water [29]. Elemental maps of the magnesium-enriched zone (Fig. 13) show severe decalcification and leaching in this zone. This is also confirmed by the elemental profiles in Figs. 14 and 15 showing a decrease in the calcium level where the magnesium level increases. It has been observed by others [23,26,28] that magnesium was only incorporated in the C–S–H after decalcification had already decomposed the C–S–H to a large extent. The morphological similarities between the magnesium-enriched zone and the rest of the paste (see Fig. 13) would indicate that M–S–H forms through the substitution of magnesium with calcium in the decalcified C–S–H (Eq. (3) [1]). However, recent findings [30,31] show that the structure of M–S–H strongly differs from that of decalcified C–S–H, thereby indicating that M–S–H cannot be formed

[1] All presented simplified chemical equations are assumed to occur in excess water and should full fill the electroneutrality requirement.

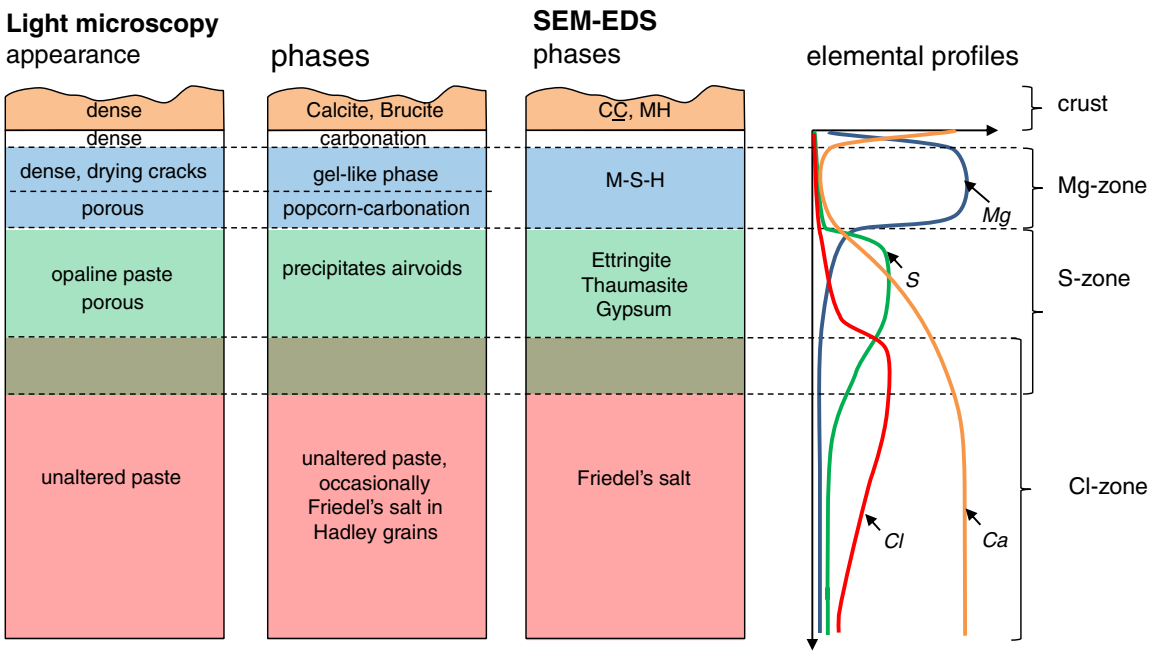

Fig. 6. Schematic overview of the different zones and the corresponding observations using light microscopy and SEM–EDS.

through ion exchange between Mg and Ca in decalcified C–S–H. A simplified chemical reaction for the formation of M–S–H is given in Eq. (3) [8].

$$C\text{–}S\text{–}H_{decalc(s)} + Mg^{2+}_{(aq)} \rightarrow M\text{–}S\text{–}H_{(s)} + Ca^{2+}_{(aq)} \quad (3)$$

Figs. 14 and 15 show calcium and magnesium profiles for sections with and without calcite crust on the surface. Magnesium values over 25 at.% typically indicate the presence of brucite, but otherwise high magnesium and low calcium levels indicate the presence of M–S–H. However, where the calcite crust was present on intact surfaces (the three concretes from Solsvik), no M–S–H zone was observed, which indicates that an initially formed calcite crust tends to prevent the formation of M–S–H.

In the optical microscope under crossed polarized light (see Figs. 16 and 10), the Mg-rich zone appears black without any sign of birefringent phases such as calcium hydroxide. The paste in the M–S–H-zone

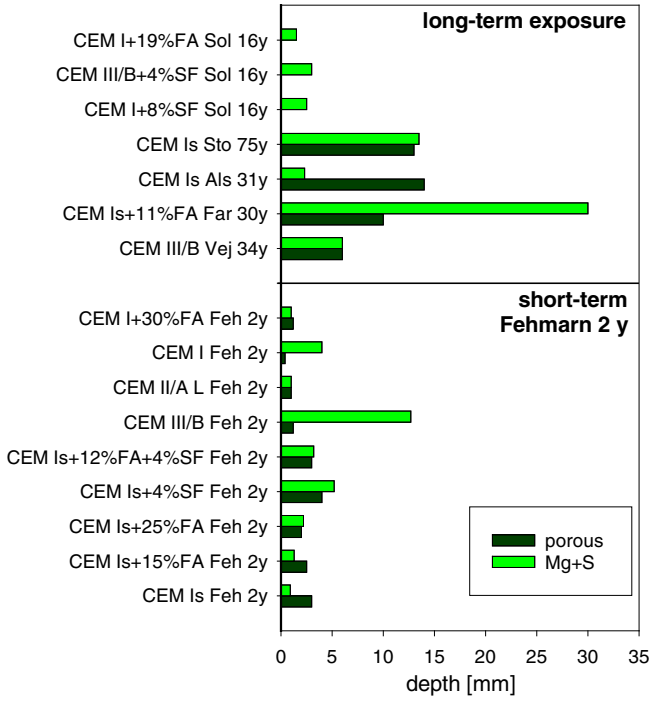

Fig. 7. Bar diagrams showing the depth of the zone with increased capillary porosity alongside the depth of the Mg + S zone. No porosity data were available for the long-term exposed concretes not included in the graph (Øst 10y and Øre 12y).

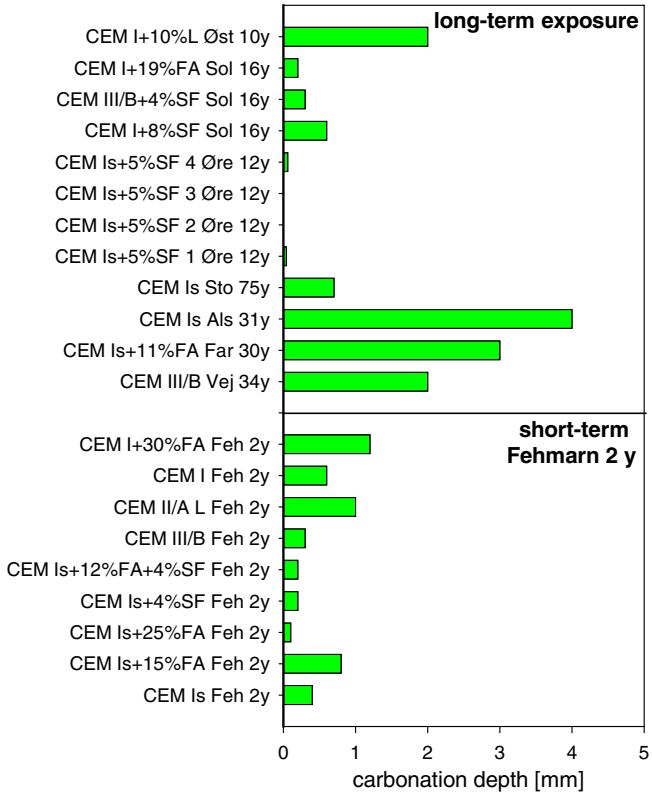

Fig. 8. Bar diagrams showing the depth of carbonation, including 'pop-corn' carbonation.

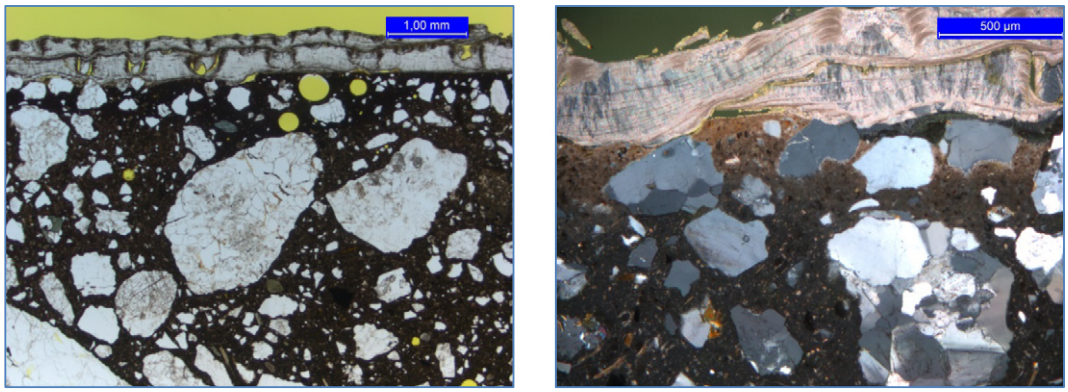

Fig. 9. Images of the calcite crust deposited on the surface of the thin section of the CEM I + 8%SF Sol 16y concrete taken with the light microscope using plane-polarized light (left) and cross-polarized light (right). The scale indicates 1.00 mm (left) and 500 µm (right). A slight carbonation of the paste (brownish) can be seen under the crust. Field of view 6 × 5 mm and 2 × 1.5 mm.

appears generally porous, and after specimen preparation, several empty, brittle cracks could be observed (10–100 µm wide).

M–S–H generally replaces decalcified C–S–H in the affected cement paste. However, in some of the samples, a special morphology of the M–S–H phase was observed using SEM–EDS. Relicts of alite grains positioned close to the exposed surface were filled with M–S–H, while the surrounding cement paste was either not or only slightly enriched with magnesium. Due to the spot-like nature of the magnesium distribution observed in the elemental mapping, this morphology was named "magnesium freckles". The reason for this specific morphology is currently not known. This feature was found especially in the Norwegian long-term exposed concretes (see Figs. 17 and 18). A similar M–S–H morphology has also been observed by Brown and Doerr in concrete samples exposed to aggressive magnesium-containing soils [29] and in the 1990'ies by the first author in California.

The composition of the M–S–H was determined using EDS point analysis for a selection of the field-exposed samples. Fig. 19a) shows the Mg/Ca ratio as a function of the Si/Ca ratio. Assuming that the M–S–H has a constant Mg/Si ratio and does not contain calcium, the point analysis results should gather along a line due to the varying extent of intermixing with Ca-containing phases in the volume analyzed by EDS. The slope of the line would relate to the Mg/Si ratio of the M–S–H. In Fig. 19a) the two dotted lines indicate the lower limits of the Mg/Si ratio: for the Solsvik (CEM III/B + 4%SF Sol 16y) and Farø Bridge concretes (CEM Is + 11%FA Far 30y), the slope is approximately 1, whereas for the short-exposure Fehmarn concrete (CEM Is + 25%FA Feh 2y) the slope is 0.5. The points which lie above the dotted lines, i.e. with a higher Mg/Si ratio, might indicate a fine intermixing of brucite with the M–S–H. The lower limit of the Mg/Si ratio or upper limit of the Si/Mg can also be read from Fig. 19c. Fig. 19b shows the Mg/Ca ratio as a function of the Al/Ca ratio. This type of plot is generally used to identify hydrotalcite by checking whether points gather along a line with a slope of 2 [32,33]. The EDS points in Fig. 19b do not gather along a single line, but they lie between lines with slopes of approximately 0.05 and 0.3, indicating the limits of the Al/Mg ratio of the M–S–H. Similar Al/Mg ratio limits can also be read from Fig. 19c and d. Comparison of Fig. 19c and d shows that the points for the Fehmarn sample move to the left when calcium is included in the denominator. This indicates that the M–S–H in the Fehmarn sample (CEM Is + 25%FA Feh 2y) still contains some calcium, which may explain the low Mg/Si ratio observed in this sample. So it can be concluded that the M–S–H phases observed have an Al/Mg ratio ranging between 0.05 and 0.3. The Si/Mg ratio is approximately 1, except for the Fehmarn sample which still seems to contain some calcium. The EDS points with higher Mg/Si ratios might indicate fine intermixing of M–S–H with brucite.

Typically, the zone with increased magnesium content does not exceed a depth of more than 1 mm, except in the cores taken from two of the old bridges, Vejle Fjord Bridge (CEM III/B Vej 34y) and the Farø

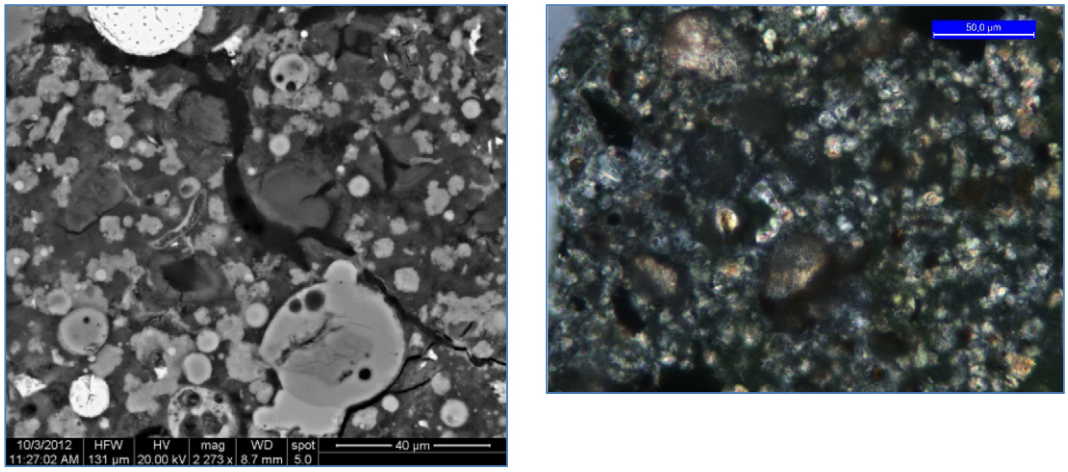

Fig. 10. Images taken in backscatter mode (left) and in cross-polarized light (right) of popcorn carbonation in the CEM Is + 25%FA Feh 2y concrete. The scale indicates 40 µm (left) and 50 µm (right). The images show the typical appearance of popcorn carbonation in the carbonated zone between the Mg- and S-zones. The "popcorn" appears as small irregular spots (not to be confused with the spherical fly-ash particles present). Field of view 131 × 131 µm and 240 × 200 µm.

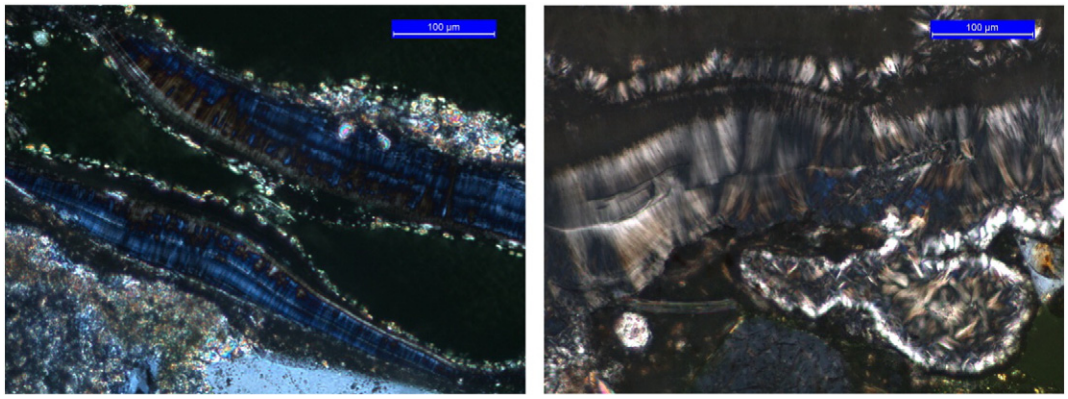

Fig. 11. Images taken in cross-polarized light of precipitated crystalline brownish to blueish wavy bands of brucite in a crack (left) and on the surface (right) of the Vilsund Bridge (1937). The scale indicates 100 µm. Field of view is 500 × 400 µm.

Bridges (CEM Is + 11%FA Far 30y), where it reached 2 and 3 mm, respectively (see Fig. 3). Brucite was observed within a calcite crust and/or in cracks in only a selection of samples, whereas M–S–H was observed in all the samples investigated; however, only limited in the 4 concretes with intact calcite crust on non-scaled surface (all concretes from Solsvik and CEM Is + 15%FA Feh 2y) (see Table 3).

3.5. Sulfate phases

Sea water is rich in sulfur (see Table 1). When hydrated cement paste is exposed to sulfur, it can lead to the formation of additional gypsum (Eq. (4)). By the reaction between sulfates and aluminate containing phases such as monosulfate additional ettringite may also form (Eq. (5)). In cases where sulfur is present in combination with $CaCO_3$, C–S–H can convert into thaumasite (Eq. (6)).

$$SO_4^{2-}(aq) + Ca(OH)_{2(s)} \rightarrow CaSO_{4(s)} + 2OH^-_{(aq)} \quad (4)$$

$$C_3A \cdot CaSO_4 \cdot 12H_2O_{(s)} + 2CaSO_{4(s)} + 20H_2O_{(l)} \rightarrow C_3A \cdot 3CaSO_4 \cdot 32H_2O_{(s)}(\text{ettringite}) \quad (5)$$

$$CaCO_{3(s)} + CaSO_{4(s)} + C{-}S{-}H_{(s)} + H_2O_{(l)} \rightarrow CaCO_3.CaSO_4.CaSiO_3.15H_2O_{(s)}(\text{thaumasite}) \quad (6)$$

The EDS dot plot shown in Fig. 4a indicates that the increased sulfur content in the OH is primarily due to the presence of ettringite finely intermixed with the C–S–H, because points seem to gather along the line connecting C–S–H and the ideal composition of ettringite. There is no trend going in the direction of gypsum. However, the crystalline phases analyzed in voids, which are included in Fig. 4b, do comprise gypsum and also thaumasite.

Fig. 20 shows a backscatter image of ettringite present in relicts of former cement grains as well as in air voids. Note, the tiny crack morphology of ettringite is not original but formed within the SEM due to dehydration of ettringite. This morphology, however, allows the operator to make an easy identification of ettringite when working with SEM–EDS analysis. The ettringite in the paste can be identified indirectly just using optical microscopy because a paste containing ettringite appears highly opaline in X-polarized light [21]. This feature is, however, not 100% proof for ettringite in paste as other phases present in the paste can give similar opaline appearance.

The formation of additional ettringite leads to an increase in the solid volume e.g. the volume of monosulfate is 309 cm^3/mol and the volume of ettringite is 746 cm^3/mol [34]. However, there is typically more porosity available compared to the additional volume taken in. There is a lack of evidence that links the expansion with the amount of ettringite formed [35]. The formation of ettringite seems to be necessary for the expansion but its volume increase does not offer the full explanation. According to the current state of the art, the degradation mechanism

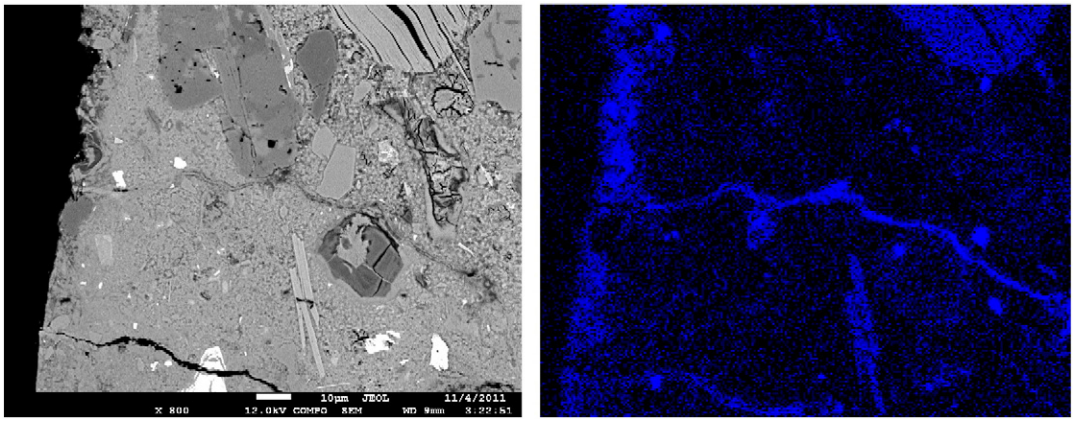

Fig. 12. Backscatter image of the surface of the CEM I + 10%L Øst 10y concrete (left) and the corresponding Mg map (right) from De Weerdt et al. [15]. Brucite is identified on the surface as well as in the cracks (bright blue colour). Field of view 115 × 151 µm and 108 × 137 µm.

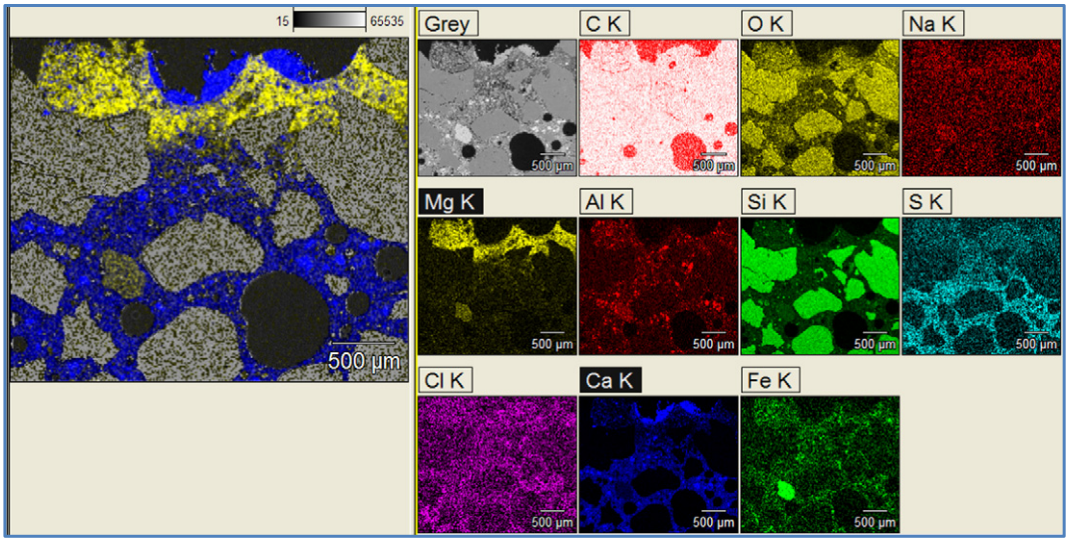

Fig. 13. EDS mapping of the surface of CEM I + 25%FA Feh 2y concrete showing the elemental distribution of Mg (yellow) and Ca (blue) on the left. The distribution of other elements present is shown on the right.

for sulfate attack is rather ascribed to crystallization pressure from a supersaturated solution [1,36].

The deleterious effect of the sulfur in sea water appears to be limited since no cracking or spalling is observed in the sulfur-rich zone. This absence of damage, despite sulfate enrichment, has been observed by other authors, e.g. Mehta [2] and Eglinton [3]. This could be attributed to the influence of the presence of other ions in the sea water on the solubility of ettringite and thereby the supersaturation of the pore solution. However this is still unclear. In the absence of damage, perhaps we should not talk about sulfate attack by sea water, but rather call it sulfur enrichment.

Not all sulfur in the sulfur-rich zone seems to originate from sea water. Part of the sulfur might move from the magnesium-rich zone and accumulate in the paste behind it, because sulfur does not adsorb onto M–S–H as it does onto C–S–H [8]. Internal movement of sulfur has been reported in unpublished work by the first author [37], from work on laboratory samples which was placed in water void of sulfur.

At temperatures below 15 °C, which are common in both Denmark and Norway, exposure to sulfate from sea water on concrete containing calcium carbonate (e.g. limestone filler) or combined sulfate and carbonate exposure from sea water on concrete can result in thaumasite formation [10,11]. Thaumasite is a non-cementing reaction product, which can result in the disintegration of the concrete. Two of the concretes examined contain limestone filler: CEM II/A L Feh 2y and CEM I + 10%L Øst 10y. From Table 3, it can be seen that thaumasite is not exclusively observed in concretes containing limestone, but it was distinctly observed in both air voids and small cracks in concrete with limestone fines from Fehmarn, CEM II/A L Feh 2y. In the other concretes, thaumasite was only occasionally observed in air voids. It was typically detected in the popcorn-carbonated zone between the M–S–H and the sulfur-rich zone. No sign of thaumasite was observed within the paste of the concretes.

The width of the sulfate-rich zone varies typically from 1 to 7 mm; however, a thickness of 27 mm was seen in the concrete from the Farø Bridges containing 11% FA (see Fig. 3). The content of sulfur in the sulfur-rich zone ranges typically from 1 to 3.5 at.% and does not show any variation related to binder type or age. The highest sulfur content of 4–5 at.% was found in two concretes, the 2-year-old concrete CEM Is + 25%FA Feh 2y from Fehmarn and the 30-year-old Farø Bridge concrete CEM Is + 11%FA Far 30y, both containing fly ash.

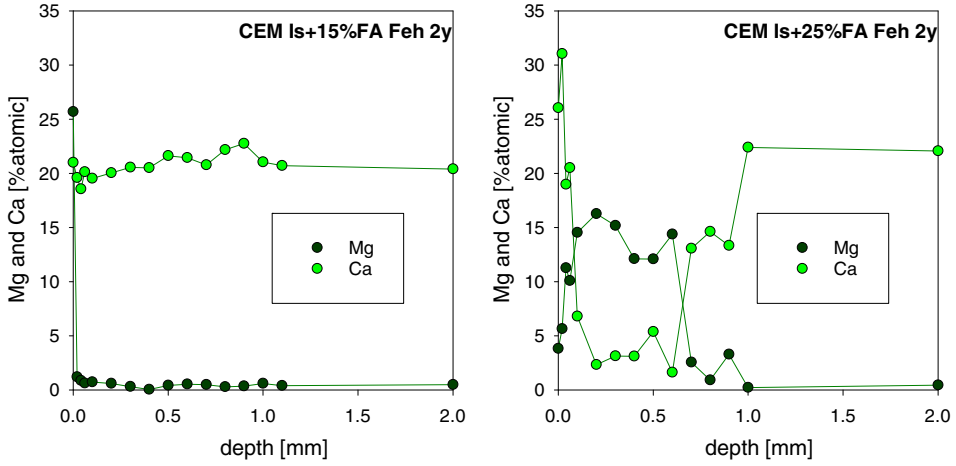

Fig. 14. SEM–EDS profiles of Mg and Ca in outer hydration product near the exposed surface for the CEM Is + 15%FA Feh 2y (left) and CEM Is + 25%FA Feh 2y (right). The former had a calcite crust and the latter not.

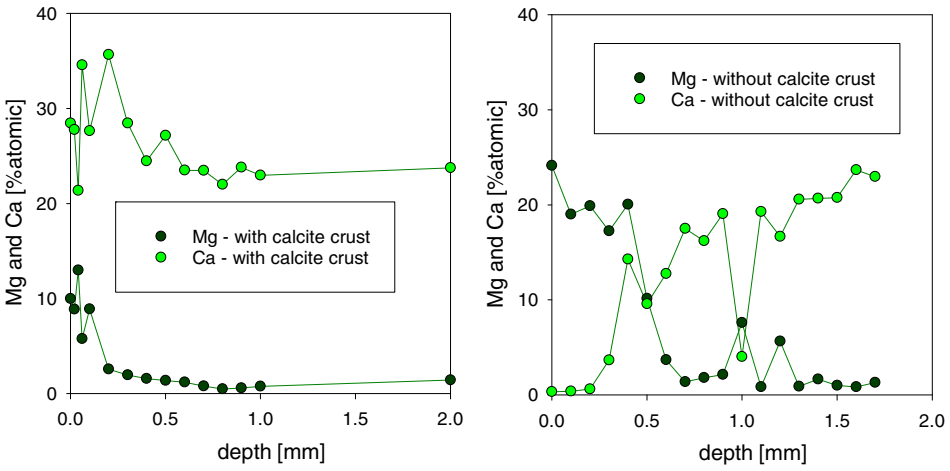

Fig. 15. SEM–EDS profiles of Mg and Ca in outer hydration product near the exposed surface for the CEM III/B + 4%SF Sol 16y concrete, part of which had a calcite crust (left), while part did not (right).

3.6. Chloride phases

In concrete, chlorine originating from sea water can be bound in hydrated cement paste in calcium chloroaluminate hydrates (see simplified Eq. (7)) or in various solid solutions between sulfate or carbonate AFm and chloride AFm [5,38]. Moreover, it can be adsorbed onto the C–S–H [6,39].

$$C_3A_{(s)} + Ca(OH)_{2(s)} + 2Cl^-_{(aq)} + 10H_2O_{(l)} \rightarrow C_3A \cdot CaCl_2 \cdot 10H_2O_{(s)} (Friedel's salt) + 2OH^-_{(aq)} \quad (7)$$

The chlorine-rich zone takes over where the sulfur-rich zone ends. In front of the zone, the chlorine content is low and close to zero. The low chlorine content in the magnesium-rich zone might be due to the low chloride-binding capacity of M–S–H and the higher solubility of chloride AFm in the low pH of this zone. In the sulfur-rich zone, the chloride binding in the paste is reduced due to preferred binding with sulfates both in AFm and C–S–H [6].

This means that the start of the chlorine zone depends on the width of the sulfur zone (Fig. 2). The maximum chlorine content in the paste follows straight after the sulfur zone. The chlorine content then gradually decreases with depth into the concrete and away from the exposed surface.

Fig. 5 shows the EDS dot plots which allow identification of the chlorine-containing phases. The cloud of points at low Al/Ca ratios can be associated with the C–S–H. These points present a range of chlorine to calcium ratios. This is related to the different depths and therefore the different chlorine contents for which the analyzes were performed. The C–S–H seems to be able to incorporate chlorine up to approximately 1.2 chlorine to calcium molar ratio. Friedel's salt and other chlorine-containing AFm phases seem to fill voids in the cement paste.

3.7. Sodium enrichment

The bar diagrams in Fig. 21 indicate a slight ingress of Na for two of the three concrete cores extracted above the average water level (CEM Is + 5%SF 1 and 2 Øre 12), but not for the third concrete from Østmarkneset (CEM I + 10%L Øst 10y) (see De Weerdt et al. [15] for further details). For the submerged samples there seems to be very limited ingress of Na; only a slight ingress is observed for the Fehmarn trial concretes CEM Is Feh 2y and CEM Is + 12%FA + 4%SF Feh 2y, and for the concrete from Vejle Fjord Bridge CEM III/B Vej 34y. This is in line with previous findings, where Na does not seem to enter into the concrete through diffusion [40,41]. However, wetting and drying of concrete, causing capillary suction, does enable Na to enter into concrete as observed by e.g. Volkwein [42]. When analyzing

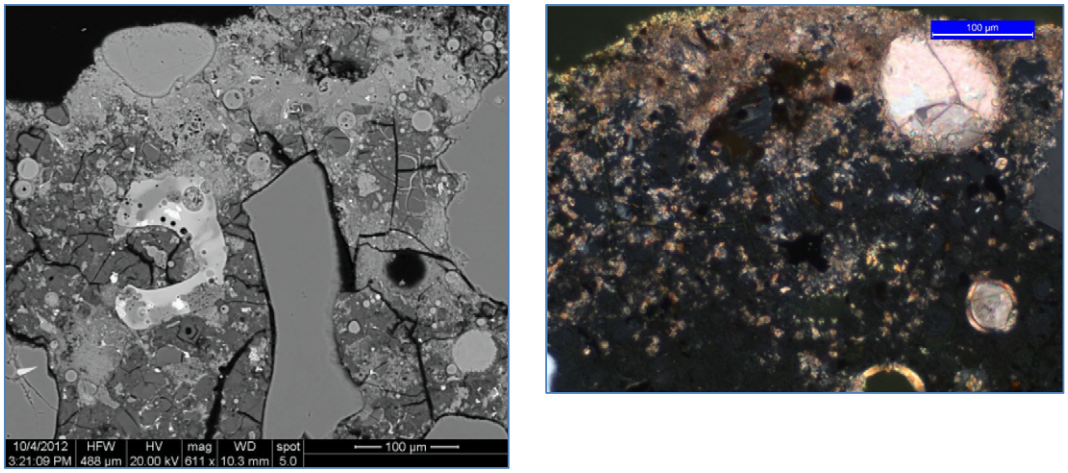

Fig. 16. Images taken of the scaled surface of Fehmarn concrete CEM Is + 12%FA + 4%SF Feh 2y in backscatter mode (left) and in cross-polarized light (right). The scales indicate 100 µm. The black paste is decalcified and consists mainly of Mg and Si (dark grey) and areas of calcite. The zone is distinctly cracked and the surface scaled. Large calcite crystals fill the air voids. Field of view 488 × 488 µm and 500 × 400 µm.

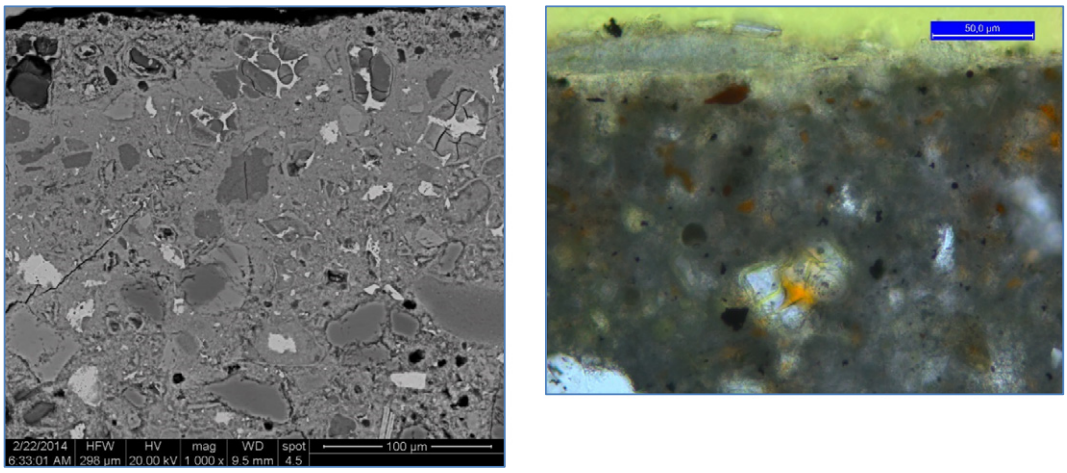

Fig. 17. Backscatter image of the Solsvik concrete CEM I + 5%SF Sol 16y (left). Near the exposed surface, a dark grey phase is observed in relicts of alite grains in the cement ('freckles'). This phase is M–S–H. In the optical microscope (right), the freckles are identified by a change in the colour from dark brown to orange of the ferrite surrounding the former grains of alite. Field of view 295 × 295 µm and 240 × 200 mm.

sodium profiles, the limited binding capacity of the cement hydrates leading to relatively lower contents than e.g. chlorine should be kept in mind.

3.8. Surface scaling (self-peeling)

Visual examination of the concretes indicates that, in general, none of the tested concretes displayed any major damage on the surface, though minor loss of the cement paste is common (Table 3). It should be kept in mind that the cores were taken from visually intact areas, and that the concretes were not exposed to abrasion, except for the concrete from Østmarkneset in the tidal zone of Trondheim Fjord.

The formation of phases with low cementing properties, e.g. M–S–H and thaumasite, and voluminous phases, e.g. ettringite, could lead to the deterioration of the surface. However, the absence of macroscopic damage indicates that the phase changes observed only lead to minor scaling, due to the low strength of the M–S–H phase.

The formation of a calcite crust seems to have a protective effect on the underlying concrete, because it seems to prevent the formation of M–S–H, which is known to have low cementing properties and could lead to loss of material when concrete in a marine environment is subjected to abrasion.

4. Conclusion

Microstructural analysis has revealed the presence of chemical and mineralogical zonation in the surface region of marine-exposed concrete. The order of the zones was independent of the age, exposure and binder composition. In addition to the zonation, the precipitation of a crust of calcite potentially intermixed with brucite was observed on the surface of some of the concretes investigated. No macroscopic damage was observed in the concretes investigated.

Using the EDS analysis, the following observations were made about the zones in the concrete:

1. The outermost zone of the concrete, typically 1–3 mm wide, is slightly cracked, decalcified and rich in magnesium. The zone consists mainly of M–S–H. Brucite is only occasionally present.

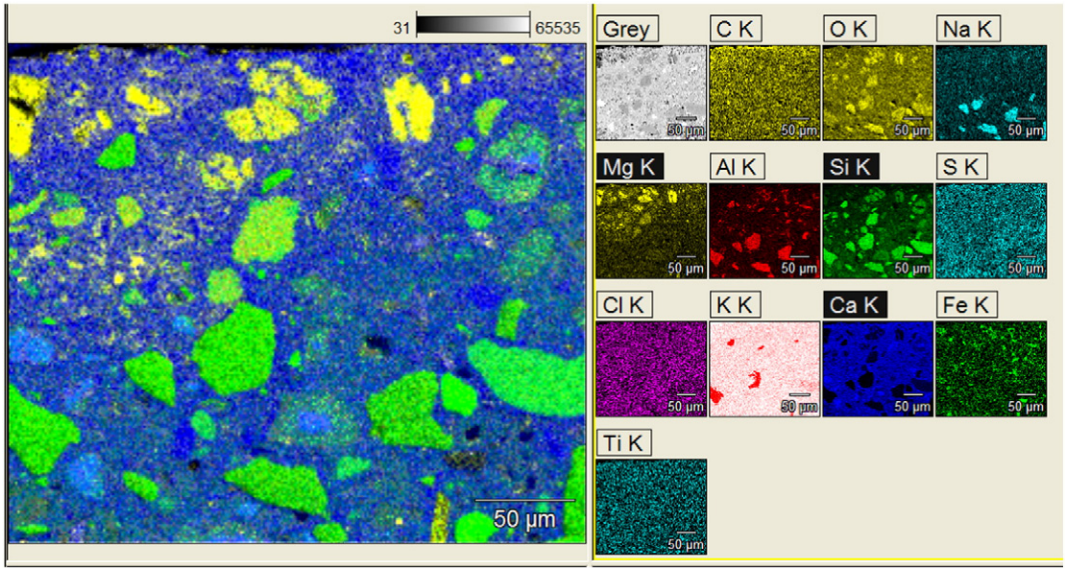

Fig. 18. EDS mapping of the surface of Solsvik concrete CEM I + 5%SF Sol 16y showing the elemental distribution of Mg (yellow), Ca (blue) and Si (green) on the left. The elemental maps reveal the presence of a magnesium rich phase in relics of alite grains. The distribution of other elements present is shown on the right.

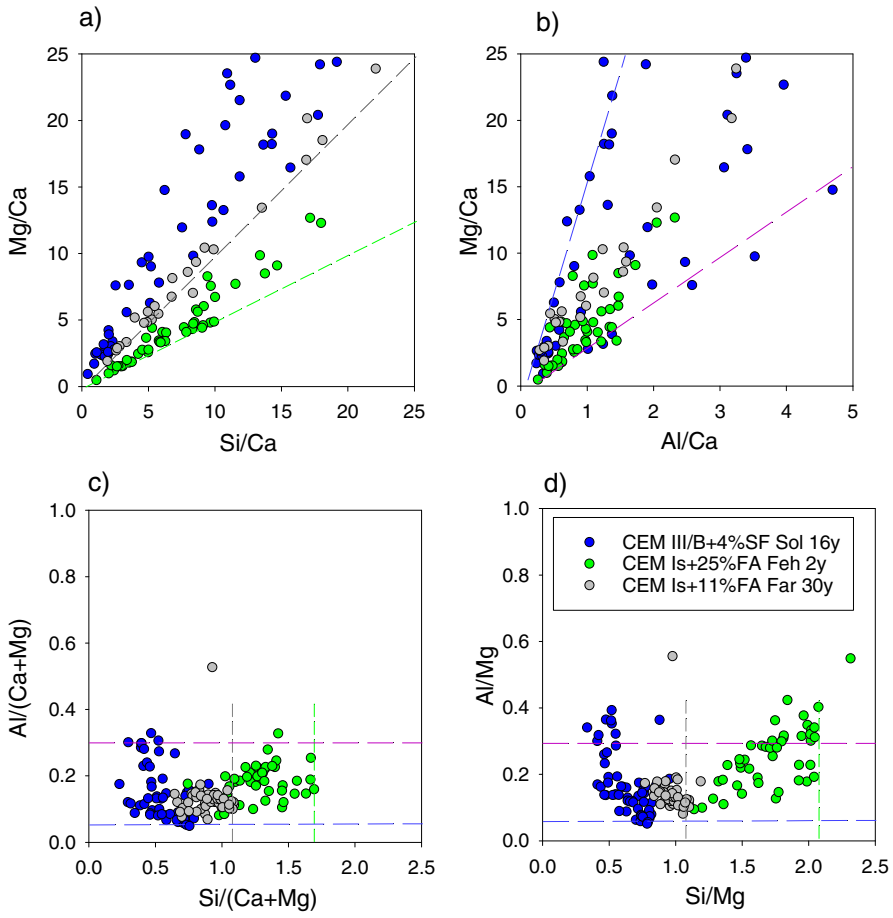

Fig. 19. SEM–EDS plots of M–S–H in matrix and as freckles in three different concretes (Solsvik concrete CEM I + 5%SF Sol 16y, the Farø Bridges CEM Is + 11%FA Far 34y, and Fehmarn CEM Is + 25%FA Feh 2y). The green and black dotted lines indicate the lower limits of Mg/Si for the Fehmarn and for the Solsvik and Farø concretes, respectively. The red and blue lines indicate the limits of Al/Mg in the M–S–H.

2. Behind the magnesium-rich zone, a sulfur-rich zone occurs. Typically 1–7 mm wide, it contains distinct amounts of ettringite in relicts after former alite grains. Occasionally thaumasite and gypsum occur in air voids within this zone.
3. Behind the sulfur-rich zone, a chlorine-rich zone is found with chlorine present in C–S–H and in Friedel's salt.

5. Perspectives

The absence of macroscopic damage suggests that the phase changes observed lead to none or only minor scaling. This is independent of whether the binders of the concretes are sulfate-resistant or not, and therefore indicates that, rather than sulfate attack, sea water seems to

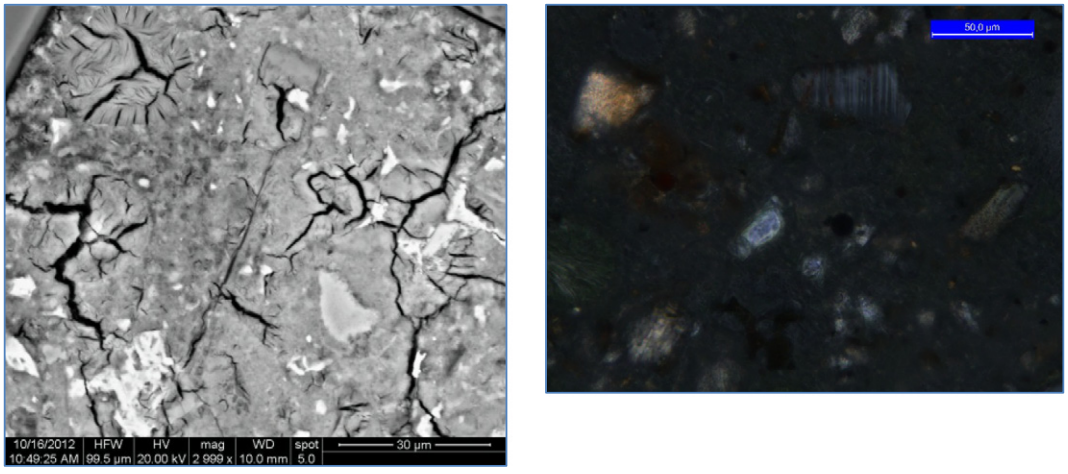

Fig. 20. Images taken of the S-zone of the Fehmarn concrete CEM Is Feh 2y in backscatter mode (left) and in cross-polarized light (right). The scale indicates 30 (left) and 500 µm (right). The S-zone behind the Mg-zone is decalcified and very rich in ettringite in e.g. air voids and relicts after cement grains. In cross-polarized light, the paste appears black with an opaline shine. This zone occasionally contains thaumasite and gypsum in air voids. Note that the cracking of ettringite is an artefact formed during SEM due to dehydration/shrinkage of the H_2O-rich phase. Field of view 100 × 100 µm and 240 × 200 µm.

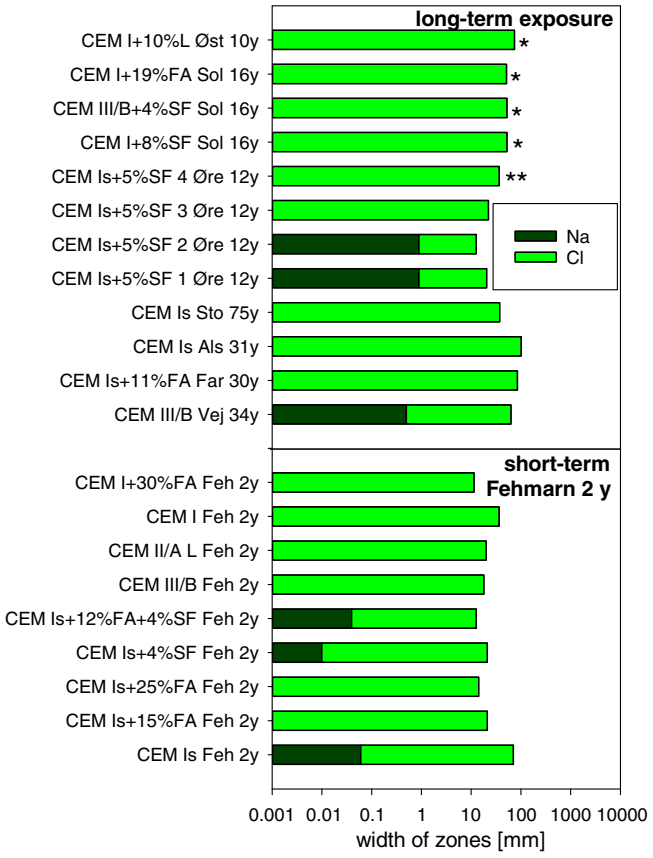

Fig. 21. Bar diagrams comparing the ingress depth of Na with that of Cl in the concretes tested. (*) indicates that the end of the chloride-rich zone was determined by titration; (**) indicates high chloride at the end of the section.

cause mere sulfur enrichment. In the light of this, the need for specifical sulfate-resistant cements in concrete subjected to marine exposure in Scandinavia could be questioned. However, it should be noted that the samples tested were taken from visually intact parts of the structures; they do not take into account the potential impact of defects and inhomogeneities from the construction stage.

Phase changes in the concrete surface in the form of enrichment in magnesium and sulfur as well as substantial leaching reduce the chloride-binding capacity of the concrete and move the maximum chloride concentration deeper into the sample. On the other hand, partial leaching increases the chloride-binding capacity, thus causing a time-dependent increase in the maximum chloride content [43]. These phase changes are part of the explanation for the apparent time dependency of the chloride diffusion coefficient and what is known as the surface concentration of chloride in concrete [44]. Ongoing work will focus on the implementation of these findings for the improvement of models and input data for chloride ingress prediction. A procedure for calculating the chloride diffusion coefficient and surface concentration from a profile with a maximum close to the concrete surface has recently been proposed by Andrade et al. [45]. The concept has also been presented by De Weerdt et al. in Ref. [43], and it resembles the suggestions in *fib* Model Code For Service Life Design 2006 [46] on how to exclude a possible convection zone.

The observed partial filling of air voids by precipitation of e.g. calcite and ettringite might affect the long-term frost resistance of concrete.

Acknowledgments

The authors would like to acknowledge COIN, the COncrete INnovation center (www.coinweb.no), Femern Bælt A/S, Sund & Bælt Holding A/S, the Danish Expert Centre for Infrastructure Constructions, and the Danish Technological Institute (DTI) for facilitating this collaboration project between the Norwegian University for Science and Technology (NTNU) and the DTI.

References

[1] W. Kunther, B. Lothenbach, K.L. Scrivener, On the relevance of volume increase for the length changes of mortar bars in sulfate solutions, Cem. Concr. Res. 46 (2013) 23–29.
[2] P.K. Mehta, Chapter 5: Causes of Deterioration of Concrete in Seawater, Concrete in the Marine Environment, Routledge, Taylor & Francis Books, Inc., 2003
[3] M. Eglinton, Resistance of concrete to destructive agencies, in: P. Hewlett (Ed.), Lea's Chemistry of Cement and Concrete, fourth ed.Arnold, London 1998, pp. 299–340.
[4] H. Zibara, Binding of External Chlorides by Cement Paste, University of Toronto, National Library of Canada, Department of Civil Engineering, 2001.
[5] M. Balonis, B. Lothenbach, G. Le Saout, F.P. Glasser, Impact of chloride on the mineralogy of hydrated Portland cement systems, Cem. Concr. Res. 40 (2010) 1009–1022.
[6] K. De Weerdt, D. Orsáková, M.R. Geiker, The impact of sulphate and magnesium on chloride binding in Portland cement paste, Cem. Concr. Res. 65 (2014) 30–40.
[7] N.R. Buenfeld, J.B. Newman, The development and stability of surface layers on concrete exposed to sea-water, Cem. Concr. Res. 16 (1986) 721–732.
[8] K. De Weerdt, H. Justnes, The effect of sea water on the phase assemblage of hydrated cement paste, Cem. Concr. Compos. 55 (2015) 215–222.
[9] U.H. Jakobsen, Microstructural surface deterioration of concrete exposed to seawater: results after 2 years exposure, in: U.H. Jakobsen (Ed.), Proceedings of the 14th Euroseminar on Microscopy Applied to Building Materials, Helsingør, Denmark 2013, pp. 62–66.
[10] T. Sibbick, D. Fenn, N. Crammond, The occurrence of thaumasite as a product of seawater attack, Cem. Concr. *compos.* 25 (2003) 1059–1066.
[11] I. Juel, Mineralogical and Thermodynamic Processes by Sulfate and Seawater Attack of Danish Concrete, Geological Institute, University of Copenhagen, Faculty of Science, 2002.
[12] R. Duval, H. Hornain, Chapter 9: La durabilité des bétons vis-à-vis des eaux agressives, in: J. Baron, J.P. Ollivier (Eds.),Durabilité des bétons, Presses de l'École Nationale Des Ponts et Chaussées 1992, pp. 351–394.
[13] J. Marchand, E. Samson, D. Burke, P. Tourney, N. Thaulow, S. Sahu, Predicting the microstructural degradation of concrete in marine environment, ACI Special Publication SP-212-69 (2003) 1127–1153.
[14] A. Chabrelie, E. Gallucci, K. Scrivener, U. Müller, Durability of Field Concretes Made of Portland and silica fume cements under sea water exposure for 25 years, in: D.H. Bager (Ed.), Nordic Exposure Sites — Input to Revision of EN206-1, Workshop Proceeding from a Nordic Miniseminar, Hirtshals — Denmark, 2008.
[15] K. De Weerdt, H. Justnes, M.R. Geiker, Changes in the phase assemblage of concrete exposed to sea water, Cem. Concr. *compos.* 47 (2014) 53–63.
[16] E.J. Pedersen, CEB No. 182, Durable Concrete Structures. in: Edt Rostam Steen (Ed.), Appendix A. Curing of Concrete Structures., 1992.
[17] EN 197-1: 2011 — Part 1: composition, specifications and conformity criteria for commen cements, 2011.
[18] K. De Weerdt, M.R. Geiker, D. Orsakova, Investigation of Concrete from Solsvik Field Station — 4 Concrete Cores Investigated after 16 Years of Submerged Exposure, Statens Vegvesens Rapporter, Norwegian Public Roads Administration, Oslo, 2015.
[19] U.H. Jakobsen, P. Laugesen, N. Thaulow, Determination of water to cement ratio in hardened concrete by optical fluorescence microscopy, in: M.S. Khan (Ed.), Water–Cement Ratio and Other Durability Parameters — Techniques for Determination, ACI 2000, pp. 27–41.
[20] R.J. Detwiler, L.J. Powers, U.H. Jakobsen, W.U. Ahmed, K.L. Scrivener, K.O. Kjellsen, Preparing specimens for microscopy, Concr. Int. 23 (2001) 51–58.
[21] N. Thaulow, U.H. Jakobsen, Sulphate Attack as Observed by Optical and Scanning Electron Microscopy, Cement and Concrete Technology in the 2000s, Second International Symposium, Istandbul, Turkey, 2000.
[22] W.F. Cole, A crystalline hydrated magnesium silicate formed in the breakdown of a concrete sea-wall, Nature 171 (1953) 354–355.
[23] D. Bonen, Composition and appearance of magnesium silicate hydrate and its relation to deterioration of cement-based materials, J. Am. Ceram. Soc. 75 (1992) 2904–2906.
[24] D. Bonen, M.D. Cohen, Magnesium sulfate attack on Portland cement paste — I. Microstructural analysis, Cem. Concr. Res. 22 (1992) 169–180.
[25] D. Bonen, M.D. Cohen, Magnesium sulfate attack on Portland cement paste — II. Chemical and mineralogical analyses, Cem. Concr. Res. 22 (1992) 707–718.
[26] R.S. Gollop, H.F.W. Taylor, Microstructural and microanalytical studies of sulfate attack. I. Ordinary Portland cement paste, Cem. Concr. Res. 22 (1992) 1027–1038.
[27] H. Justnes, J.M. Østvik, Effect of magnesium chloride as a dust binder on tunnel concrete paving, in: R.K. Dhir (Ed.), Concrete Durability: Achievement and Enhancement — Proceedings of the 7th International Congress on "Concrete: Construction's Sustainable Option", IHS BRE Press, Dundee, Scotland, 2008.
[28] W. Kurdowski, The protective layer and decalcification of C–S–H in the mechanism of chloride corrosion of cement paste, Cem. Concr. Res. 34 (2004) 1555–1559.
[29] P.W. Brown, A. Doerr, Chemical changes in concrete due to the ingress of aggressive species, Cem. Concr. Res. 30 (2000) 411–418.
[30] D. Nied, K. Enemark-Rasmussen, E. L'Hopital, J. Skibsted, B. Lothenbach, Properties of magnesium silicate hydrates (M–S–H), Cem. Concr. Res. 79 (2016) 323–332.
[31] C. Roosz, S. Grangeon, P. Blanc, V. Montouillout, B. Lothenbach, P. Henocq, E. Giffaut, P. Vieillard, S. Gaboreau, Crystal structure of magnesium silicate hydrates (M–S–H): the relation with 2:1 Mg–Si phyllosilicates, Cem. Concr. Res. 73 (2015) 228–237.

[32] R.S. Gollop, H.F.W. Taylor, Microstructural and microanalytical studies of sulfate attack. IV. Reactions of a slag cement paste with sodium and magnesium sulfate solutions, Cem. Concr. Res. 26 (1996) 1013–1028.
[33] M.B. Haha, B. Lothenbach, G. Le Saout, F. Winnefeld, Influence of slag chemistry on the hydration of alkali-activated blast-furnace slag — part I: effect of MgO, Cem. Concr. Res. 41 (2011) 955–963.
[34] M. Balonis, F.P. Glasser, The density of cement phases, Cem. Concr. Res. 39 (2009) 733–739.
[35] H.F.W. Taylor, C. Famy, K.L. Scrivener, Delayed ettringite formation, Cem. Concr. Res. 31 (2001) 683–693.
[36] J. Bizzozero, C. Gosselin, K.L. Scrivener, Expansion mechanisms in calcium aluminate and sulfoaluminate systems with calcium sulfate, Cem. Concr. Res. 56 (2014) 190–202.
[37] U.H. Jakobsen, Microscopic Analysis of Samples Subjected to NaCl Solution, Teknokogisk Institut, Taastrup, Denmark, 2014.
[38] A. Mesbah, J.-P. Rapin, M. Francois, C. Cau-dit-Coumes, F. Frizon, F. Leroux, G. Renaudin, Crystal structure and phase transition of cementitious bi-anionic AFm-(Cl^-, CO_3^{2-}) compounds, J. Am. Ceram. Soc. 94 (2011) 262–269.
[39] K. De Weerdt, A. Colombo, L. Coppola, H. Justnes, M.R. Geiker, Impact of the associated cation on chloride binding of Portland cement paste, Cem. Concr. Res. 68 (2015) 196–202.
[40] E.P. Nielsen, J. Thrysøe, D. Herfort, M.R. Geiker, Performance of white Portland cement in aggressive environment, Proceedings of 7th International Conference on Concrete in Hot and Aggressive Environments Bahrain, 2003.
[41] E.P. Nielsen, The Durability of White Portland Cement to Chemical Attack, Department of Civil Engineering, Technical University of Denmark, 2004.
[42] A. Volkwein, Untersuchungen über das eindringen von Wasser und Chlorid in Beton (Investigations on the penetration of water and chlorides in concrete), Beton-Stahlbetonbau 88 (1993) 223–226.
[43] K. De Weerdt, S.G. Ytterdal, M.R. Geiker, On the impact of phase changes on chloride profiles in concrete, Proceedings of XXII Nordic Concrete Research Symposium, Reykjavik, Iceland, 2014.
[44] M.R. Geiker, K. De Weerdt, K. Hornbostel, M.M. Kioumarsi, M. Hendriks, C.K. Larsen, U. Angst, Prediction of reinforcement corrosion in concrete structures, The 1st Concrete Innovation Conference, Tekna, Oslo, Norway, 2014.
[45] C. Andrade, M.A. Climent, G. de Vera, Procedure for calculating the chloride diffusion coefficient and surface concentration from a profile having a maximum beyond the concrete surface, Mater. Struct. 48 (2015) 863–869.
[46] Fédération International Du Béton, Model Code for Service Life Design — Bulletin 34, Fib, 2006 116.
[47] A. Demayo, Elements in sea water, in: D.R. Lide (Ed.), CRC Handbook of Chemistry and Physics, CRC Press, U.S.A., 1992 (14-10).
[48] A.D. Herholdt, C.F.P. Justesen, P. Nepper-Christensen, A. Nielsen, Beton bogen, Aalborg Portland, 1979.